J Stat Phys (2007) 129: 377–405
DOI 10.1007/s10955-007-9371-4

Reaction Rate of Small Diffusing Molecules on a Cylindrical Membrane

Ronny Straube · Michael J. Ward · Martin Falcke

Received: 24 November 2006 / Accepted: 24 June 2007 / Published online: 4 August 2007

Abstract Biomembranes consist of a lipid bi-layer into which proteins are embedded to fulfill numerous tasks in localized regions of the membrane. Often, the proteins have to reach these regions by simple diffusion. Motivated by the observation that IP_3 receptor channels (IP_3R) form clusters on the surface of the endoplasmic reticulum (ER) during ATP-induced calcium release, the reaction rate of small diffusing molecules on a cylindrical membrane is calculated based on the Smoluchowski approach. In this way, the cylindrical topology of the tubular ER is explicitly taken into account. The problem can be reduced to the solution of the diffusion equation on a finite cylindrical surface containing a small absorbing hole. The solution is constructed by matching appropriate 'inner' and 'outer' asymptotic expansions. The asymptotic results are compared with those from numerical simulations and excellent agreement is obtained. For realistic parameter sets, we find reaction rates in the range of experimentally measured clustering rates of IP_3R. This supports the idea that clusters are formed by a purely diffusion limited process.

Keywords Diffusion limited reaction · Cluster rate · Asymptotic matching · Singularly perturbed domains · Regular part of the Green's function

R. Straube (✉) · M. Falcke
Abteilung Theoretische Physik, Hahn-Meitner-Institut Berlin, Glienicker Str. 100, 14109 Berlin, Germany
e-mail: ronny.straube@hmi.de

Present address:
R. Straube
Department of Systems Biology, Max-Planck-Institute for Dynamics of Complex Technical Systems, Sandtorstr. 1, 39106 Magdeburg, Germany
e-mail: rstraube@mpi-magdeburg.mpg.de

M.J. Ward
Department of Mathematics, University of British Columbia, Vancouver, BC, V6T 1Z2, Canada

1 Introduction

The endoplasmic reticulum (ER) is a nucleus associated organelle with a tubular network structure found in nearly all eucariotic cells. It is the site where proteins are translated, folded and transported. In addition, the ER is one of the main intracellular stores for calcium ions. Ca^{2+} is a second messenger translating extracellular stimuli into intracellular responses, e.g. in the form of homogeneous oscillations of the calcium concentration. Different stimuli are coded in the shape, amplitude and, or, frequency of the oscillations [4, 16]. Ca^{2+} is released through IP_3R (inositol 1,4,5-trisphosphate) receptor channels, which are integral membrane proteins of the ER. The open probability of IP_3R depends on the Ca^{2+} concentration on the outside of the storage compartment from which Ca^{2+} is released. Therefore, the channels communicate by Ca^{2+} diffusion outside the ER. The strength of coupling depends on channel distance. Recently, Tateishi et al. [22] reported that clustering of IP_3R receptor channels on the ER membrane can be (reversibly) induced by IP_3-generating agents such as extracellular ATP. In particular, they argued that clustering is induced by the conformational change of the IP_3R protein to its open state.

Clustering of membrane receptors is a common phenomenon that has received considerable attention during the last decades due to its potential relevance for signal transduction processes [1, 2, 7, 9, 10, 20]. Berg and Purcell [1] showed that cells can optimally sense their environment for signaling molecules if the corresponding receptor proteins are evenly distributed over the cell surface while the receptor size should be small compared to the distance between receptors. In particular, receptor clustering was shown to reduce the sensitivity to external stimuli. In contrast, Gopalakrishnan et al. [10] argued that receptor clustering can significantly reduce the effective dissociation rate of ligand molecules by increasing the probability of immediate rebinding. As a result, the duration of interaction between the signaling and the receptor molecule is prolonged which might affect the generation of secondary signals.

The configuration of channels and clusters is of outstanding importance for intracellular Ca^{2+} release through IP_3R receptor channels ([4] and references therein). The specific configuration of channels within a cluster affects the properties of elemental release events which are the spontaneous opening of channels of a single cluster (called puffs). The average cluster distance is an important determinant for wave velocities, oscillation periods and almost all other spatio-temporal phenomena [4]. Tateishi et al. [22] have observed that clustering is a dynamic process where single receptor molecules, while diffusing along the membrane, can stick together upon encounter and thereby create 2-, 3- and eventually n-size clusters. On the other hand, as soon as the IP_3 producing agonist ATP is removed from the extracellular solution, clusters begin to break up and finally disappear. As yet, the dynamic process of clustering of IP_3R channels has not been taken into account in the modeling of calcium release events from the ER. As a first step towards a more realistic modeling we calculate the reaction rate of small diffusing molecules (IP_3R) on the membrane of the ER by explicitly taking into account that the tubular ER is a finite object and exhibits cylindrical topology.

The classical approach of calculating reaction rates dates back to Smoluchowksi [21]. He considered an ensemble of particles each of which performs a random walk in infinite space. It is assumed that as soon as two particles approach each other a reaction takes place such that the diffusion is the overall reaction rate limiting process. The diffusion limited reaction rate for spherical molecules in infinite space can be calculated as follows: A single particle of radius R is placed at the origin. In the continuum limit the random walk of the remaining

molecules is described by the diffusion equation

$$\partial_t c = D\Delta c$$

subject to the boundary conditions

$$c(R) = 0, \qquad \lim_{r\to\infty} c(r) = c_0,$$

where c is the concentration of the remaining particles, D is their diffusion coefficient and c_0 is the initial concentration, which is kept fixed at spatial infinity. The latter condition ensures that the reaction rate becomes stationary as $t \to \infty$. The absorbing boundary condition accounts for the fact that the particle located at the origin acts as a perfect sink for the remaining ones. The reaction rate is given by the integrated flux to the absorbing particle

$$k(t) = D\int_S \nabla c|_{r=R} \cdot \mathbf{n} dS, \tag{1}$$

where $\mathbf{n}$ is the outward pointing normal to the surface S of the particle. This reaction rate is a measure of the number of particles that approach the particle located at the origin per second.

In infinite three-dimensional space the reaction rate is given by [21]

$$k(t) = 4\pi DRc_0\left(1 + \frac{R}{\sqrt{\pi Dt}}\right),$$

so that in the long-time limit the stationary reaction rate $k = 4\pi DRc_0$ is approached. In contrast, in infinite two-dimensional space the reaction rate is independent of the radius, and is given to leading order by [19]

$$k(t) \sim \frac{4\pi Dc_0}{\ln t},$$

which slowly decays to zero as $t \to \infty$. This reflects the different recurrence properties of random walks in two- and three-dimensional space. While in two dimensions the probability of capturing a particle that starts a random walk at some distance $r > R$ is equal to unity, there is a finite probability in three dimensions that the particle escapes to infinity and is never captured [19].

In this paper we calculate the reaction rate of small diffusing molecules on a finite two-dimensional domain with cylindrical topology. Using an eigenfunction expansion for the solution of the diffusion equation, we show that the reaction rate decays for long times as a single exponential

$$k(t) = Ae^{-\lambda t} \tag{2}$$

where the decay rate λ has an asymptotic expansion in powers of the function $\nu = 1/\log(L/\delta)$ given by

$$\lambda = \frac{2\pi D\nu}{|\Omega_0|}(1 - 2\pi\nu R_1(\mathbf{0};\mathbf{0}) + \mathcal{O}(\nu^2)). \tag{3}$$

Here $|\Omega_0| = 4\pi LR$ is the area of the cylindrical surface, $2L$ and $2\pi R$ are its length and its circumference, respectively. Also, D is the diffusion coefficient of a molecule, while $\delta \ll L$ denotes its radius. The first order correction contains the function $R_1(\mathbf{0};\mathbf{0})$. It only depends

on the aspect ratio L/R of the cylindrical surface and thereby accounts for its particular geometry. The constant A appearing in (2) also has an asymptotic expansion. To second order it is simply given by $A = c_0|\Omega_0|\lambda$ where c_0 is the initial concentration of particles. The expansion for λ in (3) actually comprises infinitely many terms in powers of ν (cf. Sect. 3).

In Sect. 2 we formulate our problem precisely and show that the reaction rate can be obtained from a solution of the diffusion equation on a rectangular domain with a small hole at the origin augmented by appropriate boundary conditions. The hole renders the problem nontrivial and prevents us from finding an exact analytical solution. However, the small hole acts as a singular perturbation to the rectangular domain causing large but localized changes in the solution as compared to the smooth solution of the unperturbed problem. Thus, the method of asymptotic matching [13, 15, 24, 25] is used in Sect. 3 to construct an asymptotic solution of the diffusion equation from which approximate expressions for A and λ in (2) are derived. For this purpose, appropriate asymptotic expansions near the small absorbing hole (inner region) and far away from it (outer region) have to be matched. The higher order correction terms involve the function $R_1(\mathbf{0};\mathbf{0})$ which is the regular part of a certain Green's function for the rectangular domain. The regular part depends on the aspect ratio between the length and the radius of the cylindrical surface and thus, accounts for the particular geometry of the membrane. In the case of large aspect ratios, we also derive a 'non-perturbative' expression for λ in (3) which contains the logarithmic function ν in a non-polynomial way. In Sect. 4 the various asymptotic approximations are compared with corresponding results obtained from full numerical simulations. Finally, in Sect. 5 we relate our results to recent experimental observations and discuss further applications.

2 Formulation of the Problem

The ER consists of many interconnected cylindrical parts forming a tubular network. The length of a single tube is up to 5 μm while its radius varies between 0.1 and 0.5 μm. The size of IP_3R channels is about 18–30 nm. We imagine that the receptor molecules intersect the membrane surface transversely such that the intersection is a circle of radius δ (cf. Fig. 1). In the following, the extension of the receptor molecules beyond the membrane surface is neglected leading to the reduced problem of small diffusing disks on a finite cylindrical surface. In addition, we neglect the extrinsic curvature of the membrane since the size of

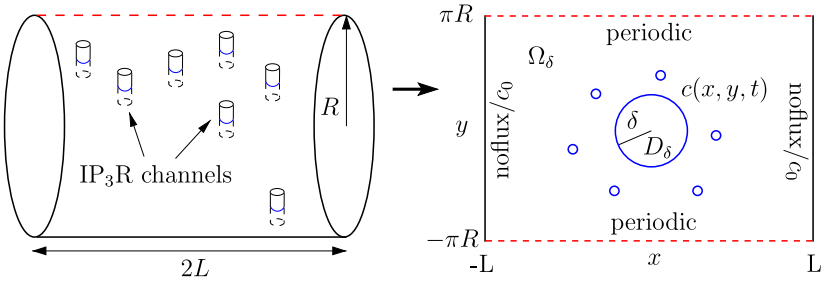

Fig. 1 Color online; Mapping the diffusion of transmembrane proteins on a cylindrical surface to diffusing disks on a rectangular domain with periodic boundary conditions at $y = \pm\pi R$ (*dashed line*). One channel is placed at the origin corresponding to the hole D_δ. The others are treated in the continuum limit by a concentration field $c(\mathbf{x}, t)$

a receptor molecule is much smaller than the length and the circumference of the cylinder. Consequently, the membrane is assumed to be locally flat. However, the cylindrical topology is accounted for by periodic boundary conditions along the circumference of the cylinder. At the bottom and top of the cylindrical surface we impose no-flux boundary conditions which corresponds to the assumption that the net flow of receptor molecules across the boundaries of an arbitrarily chosen tube of the ER meshwork is zero.

In summary, a tube of the ER membrane is modeled as a two-dimensional finite cylindrical surface Ω_δ of length $2L$ and circumference $2\pi R$ which contains a small hole of radius δ corresponding to a (fixed) receptor molecule located at the origin (cf. Fig. 1), i.e.

$$\Omega_\delta = \Omega_0 \setminus D_\delta,$$

with

$$\Omega_0 := \{(x, y) : |x| \le L, |y| \le \pi R\}, \qquad D_\delta := \{(x, y) : x^2 + y^2 \le \delta^2\}.$$

We wish to solve the diffusion equation

$$\partial_t c(\mathbf{x}, t) = D\Delta c(\mathbf{x}, t), \quad (\mathbf{x}, t) \in \Omega_\delta \times \mathbb{R}_+, \tag{4}$$

with the following boundary conditions corresponding to no-flux and periodic boundary conditions in the x and y directions, respectively,

$$\begin{aligned} &\partial_x c(\pm L, y, t) = 0, \\ &c(x, \pi R, t) = c(x, -\pi R, t), \qquad \partial_y c(x, \pi R, t) = \partial_y c(x, -\pi R, t), \end{aligned} \tag{5}$$

together with an absorbing boundary condition on the small circle $C_\delta \equiv \partial D_\delta$ given by

$$c(\mathbf{x}, t) = 0, \quad \mathbf{x} \in C_\delta. \tag{6}$$

The initial condition is

$$c(\mathbf{x}, 0) = c_0, \quad \mathbf{x} \in \Omega_\delta. \tag{7}$$

In the limit $\delta \to 0$, the initial-boundary value problem (IBVP) described by (4–7), is singularly perturbed. This can be seen as follows: If $\delta = 0$, the unique solution to the problem is $c(\mathbf{x}, t) \equiv c_0$, since there are no absorbing boundaries in Ω_0 and we have imposed a homogeneous initial condition. However, for an arbitrarily small absorbing boundary ($0 < \delta \ll 1$) the solution of the IBVP will develop a boundary layer close to the absorbing circle to account for the rapid transition between the boundary value zero at C_δ and a value that is of $\mathcal{O}(1)$ in the outer region away from the hole for small times, but that eventually decays to zero as $t \to \infty$. These ideas are made more precise in the next section using a formal boundary layer theory.

3 Solution Using Asymptotic Matching

We seek a solution of (4) as an eigenfunction expansion of the form

$$c(\mathbf{x}, t; \delta) = \sum_{j=0}^{\infty} d_j^\delta \varphi_j^\delta(\mathbf{x}) e^{-\lambda_j^\delta Dt}, \quad \lambda_j^\delta \ge 0, \tag{8}$$

where the eigenfunctions φ_j^δ are solutions of the Helmholtz equation

$$\Delta\varphi_j^\delta + \lambda_j^\delta \varphi_j^\delta = 0, \quad \mathbf{x} \in \Omega_\delta, \tag{9}$$

satisfying the boundary conditions in (5) and (6). The corresponding eigenfunctions are orthonormalized as

$$\int_{\Omega_\delta} \varphi_j^\delta \varphi_k^\delta d\mathbf{x} = \delta_{jk}, \tag{10}$$

and the coefficients d_j^δ are given by

$$d_j^\delta = c_0 \int_{\Omega_\delta} \varphi_j^\delta d\mathbf{x}.$$

In terms of the eigenfunction representation (8), the problem of solving the diffusion equation is reduced to solving the eigenvalue problem (9) in the singularly perturbed domain Ω_δ. Since this problem cannot be solved exactly by standard methods, we will solve it asymptotically in the small hole limit $\delta \ll 1$.

The long-time behavior of the solution in (8) is described by the eigenmode with the smallest eigenvalue, i.e. by the first eigenpair $(\varphi_0^\delta, \lambda_0^\delta)$. Thus, for $t \gg 1$, we can approximate the solution as

$$c(\mathbf{x}, t; \delta) \sim d_0^\delta \varphi_0^\delta(\mathbf{x}) e^{-\lambda_0^\delta D t}, \quad 0 < \delta \ll 1. \tag{11}$$

To find an appropriate outer expansion, we first study the unperturbed problem corresponding to $\delta = 0$ in (9). In this case, the well-known boundary value problem

$$\Delta\psi_j = -\mu_j \psi_j, \quad \mathbf{x} \in \Omega_0; \qquad \int_{\Omega_0} \psi_i \psi_j d\mathbf{x} = \delta_{ij}$$

is obtained for the rectangular domain without a hole subject to the boundary conditions of (5). The eigenvalues $\mu_j \geq 0$ are ordered as $0 = \mu_0 < \mu_1 \leq \mu_2 \leq \cdots$, and the first normalized eigenpair (μ_0, ψ_0) is

$$\mu_0 = 0, \qquad \psi_0 = \frac{1}{|\Omega_0|^{\frac{1}{2}}}, \tag{12}$$

where $|\Omega_0|$ denotes the area of Ω_0.

For small nonzero δ, we expect for each fixed $j \geq 0$ that

$$\lambda_j^\delta \to \mu_j \quad \text{as } \delta \to 0.$$

In addition, the eigenfunctions of (9) will develop a boundary layer close to the absorbing circle C_δ where they change rapidly from the value zero at C_δ to a value of $\mathcal{O}(1)$ far away from the hole. Consequently, Ω_δ may be decomposed into an 'inner' region ($|\mathbf{x}| \sim \mathcal{O}(\delta)$) close to the absorbing boundary and an 'outer' region ($|\mathbf{x}| \gg \mathcal{O}(\delta)$) where the eigenfunctions deviate only slightly from those of the corresponding problem in the unperturbed domain Ω_0, i.e.

$$|\varphi_j^\delta - \psi_j| \ll 1, \qquad |\mathbf{x}| \gg \mathcal{O}(\delta).$$

In each of the two regions, we shall give an appropriate asymptotic expansion of the dominant eigenfunction φ_0^δ which yields a series of simpler problems that can be solved.

In particular, the eigenfunction in the outer region will satisfy the reflecting and periodic boundary conditions, while that of the inner expansion must vanish at the absorbing circle. Asymptotic matching of the expansions fixes the singularity type of the outer solution near the origin, and determines the correction terms to the unperturbed eigenvalue $\mu_0 = 0$.

3.1 Asymptotic Expansion in the Outer Region

For eigenvalue problems in a two-dimensional domain containing small circular holes of a common radius $\delta \ll 1$, and with a homogeneous Dirichlet condition imposed on the boundary of each hole, it was shown in Refs. [15, 25] that the principal eigenvalue has an infinite logarithmic expansion of the form

$$\lambda_0^\delta = \nu A_1 + \nu^2 A_2 + \nu^3 A_3 + \dots, \quad \nu \equiv -\frac{1}{\log \delta}. \tag{13}$$

In Ref. [25] a hybrid numerical method was formulated to effectively sum this infinite logarithmic expansion. Related steady-state diffusion problems with small holes were considered in Ref. [24]. Our first goal is to derive analytical formulae for A_1, A_2 and A_3 to obtain an explicit three-term expansion for λ_0^δ. In Sect. 3.5, we will also derive an infinite logarithmic expansion containing arbitrary high powers of the logarithmic gauge function $\nu(\delta)$. Both expansions will be compared with results from numerical simulations in Sect. 4.

The corresponding eigenfunction is constructed using the method of matched asymptotic expansions. In the outer region $|\mathbf{x}| \gg \mathcal{O}(\delta)$ we expand the principal eigenfunction as

$$\varphi_{0,out}^\delta(\mathbf{x}) = |\Omega_0|^{-\frac{1}{2}} + \nu \Phi_1(\mathbf{x}) + \nu^2 \Phi_2(\mathbf{x}) + \nu^3 \Phi_3(\mathbf{x}) + \cdots \tag{14}$$

which reduces to the constant solution of the unperturbed problem (12) in the limit $\delta \to 0$. Upon substituting (13) and (14) into (9), and equating powers of ν, we obtain that Φ_1 satisfies

$$\Delta \Phi_1 = -A_1 |\Omega_0|^{-\frac{1}{2}}, \quad \mathbf{x} \in \Omega_0 \setminus \{\mathbf{0}\}; \qquad \int_{\Omega_0} \Phi_1 d\mathbf{x} = 0. \tag{15}$$

The equation for Φ_2 reads

$$\begin{aligned} &\Delta \Phi_2 = -A_2 |\Omega_0|^{-\frac{1}{2}} - A_1 \Phi_1, \quad \mathbf{x} \in \Omega_0 \setminus \{\mathbf{0}\}, \\ &\int_{\Omega_0} (\Phi_1^2 + 2|\Omega_0|^{-\frac{1}{2}} \Phi_2) d\mathbf{x} = 0. \end{aligned} \tag{16}$$

Finally, at third order we obtain that Φ_3 satisfies

$$\begin{aligned} &\Delta \Phi_3 = -A_3 |\Omega_0|^{-\frac{1}{2}} - A_1 \Phi_2 - A_2 \Phi_1, \quad \mathbf{x} \in \Omega_0 \setminus \{\mathbf{0}\}, \\ &\int_{\Omega_0} (2\Phi_1 \Phi_2 + 2|\Omega_0|^{-\frac{1}{2}} \Phi_3) d\mathbf{x} = 0. \end{aligned} \tag{17}$$

The integral constraints in (15–17) are derived from the normalization condition (10) upon using the expansion in (14). Each Φ_j must satisfy the boundary conditions in (5). In addition, we will show below that upon matching to an appropriate inner expansion each Φ_j must have a certain singularity behavior as $\mathbf{x} \to \mathbf{0}$. Therefore, the origin has to be omitted in the definition of (15–17).

3.2 Asymptotic Expansion in the Inner Region

In the region near the small hole we introduce a local variable $\mathbf{y} = \delta^{-1}\mathbf{x}$ to obtain the scaled eigenvalue equation

$$\Delta_y \varphi^{\delta}_{0,in} = -\delta^2 \lambda^{\delta}_0 \varphi^{\delta}_{0,in}. \tag{18}$$

An appropriate expansion of the inner solution should vanish for fixed y in the limit $\delta \to 0$, and therefore it has the form

$$\varphi^{\delta}_{0,in} = \nu V_1(\mathbf{y}) + \nu^2 V_2(\mathbf{y}) + \nu^3 V_3(\mathbf{y}) + \cdots. \tag{19}$$

Note that the right-hand side of the scaled eigenvalue equation (18) is $\mathcal{O}(\delta^2\nu^2)$ whereas the left-hand side contains powers of the logarithmic gauge function $\nu(\delta) = -1/\log\delta$. Now, since $\delta^2\nu^2 = o(\nu^k)$ for $k \geq 1$, each of the functions $V_i(\mathbf{y})$ is a solution of Laplace's equation $\Delta_y V_i = 0$, for $|\mathbf{y}| \geq 1$, with $V_i = 0$ on $|\mathbf{y}| = 1$, which accounts for the absorbing boundary condition on C_δ. The solution is simply

$$V_i = A_i \log|\mathbf{y}|, \quad i \geq 1,$$

where the A_i, for $i \geq 1$, will be found from matching with the outer solution.

3.3 Matching Inner and Outer Expansions

Rewriting the inner expansion (19) in outer variables, and recalling that $\nu = -1/\log\delta$, we obtain the far-field expansion of the inner solution as

$$\begin{aligned}\varphi^{\delta}_{0,in}(\mathbf{x}) = A_1 + \nu(A_1 \log|\mathbf{x}| + A_2) + \nu^2(A_2 \log|\mathbf{x}| + A_3) \\ + \nu^3(A_3 \log|\mathbf{x}| + A_4) + \cdots,\end{aligned} \tag{20}$$

which must match the near-field behavior (as $\mathbf{x} \to 0$) of the outer solution given in (14). This determines the constants A_j as

$$A_1 = |\Omega_0|^{-\frac{1}{2}}; \qquad A_{j+1} = \lim_{\mathbf{x}\to\mathbf{0}}(\Phi_j(\mathbf{x}) - A_j \log|\mathbf{x}|), \quad j = 1, 2. \tag{21}$$

In addition, the matching condition yields that the functions Φ_j for $j \geq 1$ have logarithmic singularities near the origin

$$\Phi_j \sim A_j \log|\mathbf{x}|, \quad \text{as } \mathbf{x} \to \mathbf{0}, \ j = 1, 2, 3. \tag{22}$$

Since the free space Green's function $G_F = -(2\pi)^{-1}\log|\mathbf{x}|$ satisfies $\Delta G_F = -\delta(\mathbf{x})$ for $\mathbf{x} \in \mathbb{R}^2$, it readily follows that one may add in (15–17) source terms of the form $2\pi A_j \delta(\mathbf{x})$ to account for this singularity behavior of the functions Φ_j for $j \geq 1$. As a result, we get

$$\Delta\Phi_1 = -\Lambda_1|\Omega_0|^{-\frac{1}{2}} + 2\pi|\Omega_0|^{-\frac{1}{2}}\delta(\mathbf{x}), \quad \mathbf{x} \in \Omega_0, \tag{23}$$

$$\Delta\Phi_2 = -\Lambda_2|\Omega_0|^{-\frac{1}{2}} - \Lambda_1\Phi_1 + 2\pi A_2\delta(\mathbf{x}), \quad \mathbf{x} \in \Omega_0, \tag{24}$$

$$\Delta\Phi_3 = -\Lambda_3|\Omega_0|^{-\frac{1}{2}} - \Lambda_2\Phi_1 - \Lambda_1\Phi_2 + 2\pi A_3\delta(\mathbf{x}), \quad \mathbf{x} \in \Omega_0. \tag{25}$$

This shows that the small absorbing hole acts as a point source centered at the origin for the outer solution, with the strength of the source determined by the coefficients A_j for $j \geq 1$ of the inner expansion.

The eigenvalue corrections Λ_i in (23–25) are fixed by the divergence theorem in conjunction with the boundary condition in (5) on $\partial\Omega_0$, e.g.

$$\int_{\Omega_0} \Delta\Phi_1 d\mathbf{x} = \int_{\partial\Omega_0} \nabla\Phi_1 \cdot \mathbf{n} dS = \int_{\Omega_0} \left(-\frac{\Lambda_1}{|\Omega_0|^{\frac{1}{2}}} + \frac{2\pi}{|\Omega_0|^{\frac{1}{2}}} \delta(\mathbf{x}) \right) d\mathbf{x} = 0.$$

This determines Λ_1 as

$$\Lambda_1 = \frac{2\pi}{|\Omega_0|}. \tag{26}$$

In a similar way, Λ_2 and Λ_3 are obtained from (24) and (25), respectively, as

$$\Lambda_2 = \frac{2\pi}{|\Omega_0|^{\frac{1}{2}}} A_2, \tag{27}$$

$$\Lambda_3 = \frac{2\pi}{|\Omega_0|^{\frac{1}{2}}} A_3 - \frac{\Lambda_1}{|\Omega_0|^{\frac{1}{2}}} \int_{\Omega_0} \Phi_2 dx. \tag{28}$$

In the following, we wish to derive explicit expressions for the two constants A_2 and A_3. For further calculations, it is convenient to introduce the Neumann Green's function $G_1(\mathbf{x}; \mathbf{0})$ through the rescaling

$$\Phi_1 = -2\pi |\Omega_0|^{-1/2} G_1(\mathbf{x}; \mathbf{0}), \tag{29}$$

by which (23) takes the form

$$\Delta G_1(\mathbf{x}; \mathbf{0}) = \frac{1}{|\Omega_0|} - \delta(\mathbf{x}), \quad \mathbf{x} \in \Omega_0; \qquad \int_{\Omega_0} G_1(\mathbf{x}; \mathbf{0}) d\mathbf{x} = 0, \tag{30}$$

and $G_1(\mathbf{x}; \mathbf{0})$ satisfies the boundary conditions of (5). In terms of G_1, we introduce the regular part $R_1(\mathbf{x}; \mathbf{0})$ defined by

$$G_1(\mathbf{x}; \mathbf{0}) = -\frac{1}{2\pi} \log |\mathbf{x}| + R_1(\mathbf{x}; \mathbf{0}). \tag{31}$$

Upon using (29), we can express the second constant A_2 defined in (21) in terms of $R_1(\mathbf{0}; \mathbf{0})$ as

$$\begin{aligned} A_2 &= -2\pi |\Omega_0|^{-\frac{1}{2}} \lim_{\mathbf{x} \to \mathbf{0}} \left[G_1(\mathbf{x}; \mathbf{0}) + \frac{1}{2\pi} \log |\mathbf{x}| \right] \\ &= -2\pi |\Omega_0|^{-\frac{1}{2}} R_1(\mathbf{0}; \mathbf{0}). \end{aligned} \tag{32}$$

To obtain the constant A_3 we need an explicit representation of the function Φ_2. Upon substituting (26), (27), and (29), into (24), the equation for Φ_2 becomes

$$\Delta\Phi_2 = -2\pi A_2 \left(\frac{1}{|\Omega_0|} - \delta(\mathbf{x}) \right) + \frac{4\pi^2}{|\Omega_0|^{3/2}} G_1(\mathbf{x}; 0). \tag{33}$$

The solution of (33) fulfilling the boundary condition in (5) is

$$\Phi_2 = -2\pi A_2 G_1(\mathbf{x};0) - \frac{4\pi^2}{|\Omega_0|^{3/2}}(B_2 + G_2(\mathbf{x};0)), \tag{34}$$

where $G_2(\mathbf{x};0)$ satisfies

$$\Delta G_2 = -G_1, \quad \mathbf{x}\in\Omega_0; \qquad \int_{\Omega_0} G_2 d\mathbf{x} = 0, \tag{35}$$

subject to the boundary conditions of (5). The constant B_2 in (34) is obtained from the normalization condition in (16). Upon using (29) and (34), this condition yields

$$B_2 = \frac{1}{2}\int_{\Omega_0} [G_1(\mathbf{x};0)]^2 d\mathbf{x}. \tag{36}$$

An alternative expression for B_2 can be derived by using Green's second identity for G_1 and G_2 together with the boundary condition (5) for G_1 and G_2. We obtain,

$$0 = \int_{\Omega_0}(G_1\Delta G_2 - G_2\Delta G_1)d\mathbf{x} = -\int_{\Omega_0} G_1^2 d\mathbf{x} - \int_{\Omega_0} G_2\left(\frac{1}{|\Omega_0|} - \delta(x)\right)d\mathbf{x}.$$

Since $\int_{\Omega_0} G_2 d\mathbf{x} = 0$, we find that

$$B_2 = \frac{1}{2}G_2(\mathbf{0};\mathbf{0}). \tag{37}$$

According to (21), the constant A_3 is associated with the regular part of the function Φ_2. Thus, we expand Φ_2 in (34) as $\mathbf{x}\to 0$ using the singularity behavior of G_1 in (31). This yields that $\Phi_2 \sim A_2\log|\mathbf{x}| + A_3$, where

$$A_3 = -2\pi A_2 R_1(\mathbf{0};\mathbf{0}) - \frac{4\pi^2}{|\Omega_0|^{3/2}}(B_2 + G_2(\mathbf{0};\mathbf{0})). \tag{38}$$

Collecting everything together, we substitute (26), (34), and (38), into (28) to obtain

$$\Lambda_3 = \frac{2\pi}{|\Omega_0|^{1/2}}\left(-2\pi A_2 R_1(\mathbf{0};\mathbf{0}) - \frac{4\pi^2}{|\Omega_0|^{3/2}}G_2(\mathbf{0};\mathbf{0})\right). \tag{39}$$

This result is, naturally, independent of the constant B_2 that normalizes Φ_2. Finally, we replace A_2 by the expression in (32) and get

$$\Lambda_3 = \frac{8\pi^3}{|\Omega_0|}\left([R_1(\mathbf{0};\mathbf{0})]^2 - \frac{G_2(\mathbf{0};\mathbf{0})}{|\Omega_0|}\right). \tag{40}$$

In summary, we have derived the following three-term expansion for λ_0^δ

$$\lambda_0^\delta \sim \frac{2\pi\nu}{|\Omega_0|} - \frac{4\pi^2\nu^2}{|\Omega_0|}R_1(\mathbf{0};\mathbf{0}) + \frac{8\pi^3\nu^3}{|\Omega_0|}\left([R_1(\mathbf{0};\mathbf{0})]^2 - \frac{G_2(\mathbf{0};\mathbf{0})}{|\Omega_0|}\right). \tag{41}$$

Here $\nu = -1/\log\delta$, where $\delta \ll 1$ is the (dimensionless) radius of the small absorbing circle C_δ, and $|\Omega_0| = 4\pi LR$ is the area of the cylindrical surface. The regular part $R_1(\mathbf{0};\mathbf{0})$ is

obtained from the solution to (30) and (31) while the constant $G_2(\mathbf{0};\mathbf{0})$ is obtained from the solution to (35). The outer asymptotic expansion of the first eigenfunction φ_0^δ, with an error of $\mathcal{O}(\nu^3)$, is given by

$$\varphi_{0,out}^\delta(\mathbf{x}) \sim \frac{1}{|\Omega_0|^{\frac{1}{2}}} - \frac{2\pi\nu}{|\Omega_0|^{\frac{1}{2}}} G_1(\mathbf{x};\mathbf{0}) + \frac{4\pi^2\nu^2}{|\Omega_0|^{1/2}}\left(G_1(\mathbf{x};\mathbf{0})R_1(\mathbf{0};\mathbf{0}) - \frac{1}{|\Omega_0|}\left[G_2(\mathbf{x};\mathbf{0}) + \frac{G_2(\mathbf{0};\mathbf{0})}{2}\right]\right). \tag{42}$$

The corresponding inner asymptotic expansion

$$\varphi_{0,in}^\delta(\mathbf{y}) \sim \left(\frac{\nu}{|\Omega_0|^{\frac{1}{2}}} - \frac{2\pi\nu^2 R_1(\mathbf{0};\mathbf{0})}{|\Omega_0|^{1/2}}\right)\log|\mathbf{y}| + \frac{4\pi^2\nu^3}{|\Omega_0|^{1/2}}\left([R_1(\mathbf{0};\mathbf{0})]^2 - \frac{3}{2|\Omega_0|}G_2(\mathbf{0};\mathbf{0})\right)\log|\mathbf{y}|, \tag{43}$$

where $|\mathbf{y}| = \delta^{-1}|\mathbf{x}| = \mathcal{O}(1)$, is correct to $\mathcal{O}(\nu^3)$ terms.

3.4 Reaction Rate

The reaction rate can now be calculated using the inner expansion. We introduce polar coordinates ($\rho = |\mathbf{y}|$ and θ) and obtain from (1), (11), and (43), that

$$\begin{aligned} k(t) &= Dd_0^\delta e^{-\lambda_0^\delta Dt}\int_0^{2\pi}\left(\rho\frac{d}{d\rho}\varphi_{0,in}^\delta(\rho)\right)\Big|_{\rho=1} d\theta \\ &\sim 2\pi Dd_0^\delta e^{-\lambda_0^\delta Dt}\nu\left(\frac{1}{|\Omega_0|^{1/2}} + \nu A_2 + \nu^2 A_3\right). \end{aligned} \tag{44}$$

The constants A_2 and A_3 are given in (32) and (38), respectively. The coefficient d_0^δ in (44) can be estimated as follows:

$$\begin{aligned} \frac{d_0^\delta}{c_0} &= \int_{\Omega_\delta}\varphi_0^\delta d\mathbf{x} = \int_{\Omega_\delta}\psi_0 d\mathbf{x} + \int_{\Omega_\delta}(\varphi_0^\delta - \psi_0)d\mathbf{x}, \\ &= \int_{\Omega_0}\psi_0 d\mathbf{x} - \int_{\Omega_0\setminus\Omega_\delta}\psi_0 d\mathbf{x} + \int_{\Omega_0}(\varphi_0^\delta - \psi_0)d\mathbf{x} - \int_{\Omega_0\setminus\Omega_\delta}(\varphi_0^\delta - \psi_0)d\mathbf{x}, \\ &= |\Omega_0|^{1/2} + \nu\int_{\Omega_0}\Phi_1 d\mathbf{x} + \nu^2\int_{\Omega_0}\Phi_2 d\mathbf{x} + \mathcal{O}(\delta^2). \end{aligned}$$

Here, we used the outer expansion (14) as well as the facts that both ψ_0 and φ_0^δ are bounded from above in the inner region, i.e.

$$|\psi_0| \le K_1, \qquad |\varphi_0^\delta| \le K_2, \qquad |\mathbf{x}| \sim \mathcal{O}(\delta),$$

so that the integrals over the region $\Omega_0 \setminus \Omega_\delta$ near the hole are $\mathcal{O}(\delta^2)$. Next, we recall from (15) that $\int_{\Omega_0}\Phi_1 d\mathbf{x} = 0$. Then, from (34) and (37), we calculate

$$\int_{\Omega_0}\Phi_2 d\mathbf{x} = -\frac{2\pi^2}{|\Omega_0|^{1/2}}G_2(\mathbf{0};\mathbf{0}), \tag{45}$$

which shows that

$$d_0^\delta \sim c_0|\Omega_0|^{1/2}\left(1-\frac{2\pi^2\nu^2}{|\Omega_0|}G_2(\mathbf{0};\mathbf{0})\right). \tag{46}$$

Finally, upon substituting (32), (38), and (46), into (44), we obtain the following main result for the asymptotic estimate of the reaction rate:

$$k(t)\sim c_0 D|\Omega_0|\lambda_0^\delta e^{-\lambda_0^\delta Dt}\left(1-\frac{4\pi^2\nu^2}{|\Omega_0|}G_2(\mathbf{0};\mathbf{0})\right). \tag{47}$$

Here λ_0^δ, as given in (41), is accurate up to and including terms of order $\mathcal{O}(\nu^3)$. Therefore, the magnitude of the reaction rate in (47) is correct up to and including terms of order $\mathcal{O}(\nu^3)$.

3.5 Infinite Logarithmic Expansion

In Sect. 4 we will show that the reaction rate (47) derived from the three-term expansion of the previous section exhibits substantial deviations from the results of the full numerical simulations in the case of large aspect ratios $L/R \gg 1$. For this purpose, we shall now show how to derive all of the logarithmic correction terms to the unperturbed eigenvalue following the approach in [25]. As a result, a representation of the reaction rate is obtained which compares extremely well with numerical simulations even in the case of very large aspect ratios such as $L/R = 80$.

An infinite logarithmic expansion for λ_0^δ has the form

$$\lambda_0^\delta = \lambda_0^*(\nu) + o(\mu), \quad \nu \equiv -\frac{1}{\log\delta}, \tag{48}$$

where $\mu \ll \nu^k$ for any integer $k \geq 1$. To find an appropriate expansion of the inner solution near the hole, we, introduce the local variable $\mathbf{y} = \delta^{-1}\mathbf{x}$. Since the right-hand side of the scaled eigenvalue equation (18) is $\mathcal{O}(\delta^2\nu^2)$, which is asymptotically smaller than any power of ν, we will seek an infinite logarithmic expansion in the form

$$\varphi_{0,in}^\delta = \sum_{i=1}^{\infty}\nu^i V_i(\mathbf{y}).$$

Each V_i for $i \geq 1$ is a solution of Laplace's equation for $|\mathbf{y}| \geq 1$ with $V_i = 0$ on $|\mathbf{y}| = 1$. The solution to this boundary value problem is simply given by $V_i = A_i \log|\mathbf{y}|$. Therefore, we can write the inner solution compactly as

$$v(\mathbf{y},\delta) = A(\nu)\nu V_c(\mathbf{y}) + \cdots, \tag{49}$$

where the function $A(\nu)$ is to be found, and $V_c(y) = \log|\mathbf{y}|$ is the solution of $\Delta V_c = 0$ with $V_c = 0$ on $|\mathbf{y}| = 1$. Comparing (49) with the three-term expansion of the inner solution (43), we expect that $A(\nu) \sim \mathcal{O}(1)$ as $\delta \to 0$. The far-field behavior of this inner solution, written in terms of $\mathbf{x}$, is

$$v(\mathbf{y},\delta) \sim A(\nu)\nu\log|\mathbf{x}| + A(\nu). \tag{50}$$

To calculate $\lambda_0^*(\nu)$ we have to match this far-field behavior with the near-field behavior of an appropriate expansion in the outer region away from the hole, which is taken in the form

$$\varphi_0^\delta = \varphi_0^*(\mathbf{x},\nu) + o(\mu), \tag{51}$$

where $\mu \ll \nu^k$ for any integer $k \geq 1$. Substituting (48) and (51) into (9) shows that φ_0^* satisfies

$$\begin{aligned} \Delta\varphi_0^* + \lambda_0^*\varphi_0^* &= 0, \quad \mathbf{x} \in \Omega_0 \setminus \{\mathbf{0}\}, \\ \varphi_0^* &\sim A(\nu)\nu \log|\mathbf{x}| + A(\nu), \quad \mathbf{x} \to \mathbf{0}, \\ \int_{\Omega_0} (\varphi_0^*)^2 d\mathbf{x} &= 1. \end{aligned} \tag{52}$$

Proceeding along similar lines as in Sect. 3, we introduce the Green's function $G_{\lambda_0^*}(\mathbf{x};\mathbf{0})$ for the Helmholtz operator, and its regular part $R_{\lambda_0^*}(\mathbf{x};\mathbf{0})$, satisfying

$$\Delta G_{\lambda_0^*} + \lambda_0^* G_{\lambda_0^*} = -\delta(\mathbf{x}), \quad \mathbf{x} \in \Omega_0, \tag{53}$$

$$G_{\lambda_0^*}(\mathbf{x};\mathbf{0}) = -\frac{1}{2\pi}\log|\mathbf{x}| + R_{\lambda_0^*}(\mathbf{x};\mathbf{0}), \tag{54}$$

together with the boundary conditions of (5). In terms of this Green's function, $\varphi_0^*(\mathbf{x},\nu)$ is given by

$$\varphi_0^*(\mathbf{x},\nu) = -2\pi A(\nu)\nu G_{\lambda_0^*}(\mathbf{x};\mathbf{0}). \tag{55}$$

By using (54), we expand φ_0^* as $\mathbf{x} \to \mathbf{0}$ to obtain

$$\varphi_0^*(\mathbf{x},\nu) \sim A(\nu)\nu\log|\mathbf{x}| - 2\pi A(\nu)\nu R_{\lambda_0^*}(\mathbf{0};\mathbf{0}), \quad \mathbf{x} \to \mathbf{0}, \tag{56}$$

which must be compared with the required singularity behavior of φ_0^* in (52) arising from the matching condition. As a result, we obtain a transcendental equation for $\lambda_0^*(\nu)$ given by

$$R_{\lambda_0^*}(\mathbf{0};\mathbf{0}) = -\frac{1}{2\pi\nu}, \quad \nu = -\frac{1}{\log\delta}. \tag{57}$$

Finally, the amplitude $A(\nu)$ is obtained from the normalization condition

$$4\pi^2 A^2(\nu)\nu^2 \int_{\Omega_0} [G_{\lambda_0^*}(\mathbf{x};\mathbf{0})]^2 d\mathbf{x} = 1. \tag{58}$$

The solution of the Helmholtz equation (53) can be obtained in a similar way as shown in Appendix 1 for the Green's function G_1 satisfying (30). The result is

$$\begin{aligned} G_{\lambda_0^*}(\mathbf{x};\mathbf{0}) = &-\frac{1}{|\Omega_0|\lambda_0^*} + \frac{2}{|\Omega_0|}\left(\sum_{m=1}^{\infty}\frac{\cos(m\pi x)}{\pi^2 m^2 - \lambda_0^*} + \sum_{n=1}^{\infty}\frac{\cos(\frac{nL}{R}y)}{(\frac{nL}{R})^2 - \lambda_0^*}\right) \\ &+ \frac{2}{|\Omega_0|}\left(\sum_{m,n=1}^{\infty}\frac{2\cos(m\pi x)\cos(\frac{nL}{R}y)}{(m\pi)^2 + (\frac{nL}{R})^2 - \lambda_0^*}\right). \end{aligned} \tag{59}$$

Since we are interested in the case when λ_0^* only slightly deviates from the unperturbed eigenvalue $\mu_0 = 0$, the Helmholtz Green's function can be expanded for $\lambda_0^* \ll 1$ as

$$G_{\lambda_0^*}(\mathbf{x};\mathbf{0}) = -\frac{1}{\lambda_0^*|\Omega_0|} + G_1(\mathbf{x};\mathbf{0}) + \lambda_0^* G_2(\mathbf{x};\mathbf{0}) + \mathcal{O}([\lambda_0^*]^2). \tag{60}$$

Upon substituting this expression into (53) and (54) we see that G_1 and G_2 satisfy (30) and (35), respectively. Thus, they are precisely the same functions that appear in the three-term

expansion of the outer solution (42). A similar expansion of the transcendental equation (57) for λ_0^* yields

$$R_{\lambda_0^*}(\mathbf{0};\mathbf{0}) = -\frac{1}{\lambda_0^*|\Omega_0|} + R_1(\mathbf{0};\mathbf{0}) + \lambda_0^* G_2(\mathbf{0};\mathbf{0}) + \mathcal{O}([\lambda_0^*]^2) = -\frac{1}{2\pi\nu}. \tag{61}$$

Neglecting terms of $\mathcal{O}([\lambda_0^*]^2)$ and higher, we obtain a quadratic equation for λ_0^*, the relevant solution of which is given by

$$\lambda_0^* = \frac{2\pi\nu R_1(\mathbf{0};\mathbf{0})+1}{4\pi\nu G_2(\mathbf{0};\mathbf{0})}\left(\sqrt{1+\frac{1}{G_2(\mathbf{0};\mathbf{0})|\Omega_0|}\left(\frac{4\pi\nu G_2(\mathbf{0};\mathbf{0})}{2\pi\nu R_1(\mathbf{0};\mathbf{0})+1}\right)^2}-1\right). \tag{62}$$

The small argument expansion of the square root up to second order yields

$$\lambda_0^* \approx \frac{2\pi\nu}{|\Omega_0|}\frac{1}{1+2\pi\nu R_1(\mathbf{0};\mathbf{0})} - \left(\frac{2\pi}{|\Omega_0|}\right)^2 \nu^3 \frac{2\pi G_2(\mathbf{0};\mathbf{0})}{(1+2\pi\nu R_1(\mathbf{0};\mathbf{0}))^3}. \tag{63}$$

This expression can, again, be expanded provided that $|2\pi\nu R_1(\mathbf{0};\mathbf{0})| \ll 1$. A straightforward calculation shows that the three-term expansion in (63) precisely coincides with the three-term expansion appearing in (41) obtained earlier.

The reaction rate can be calculated in a similar way as in (44) using the inner expansion from (49). We obtain

$$\begin{aligned} k^*(t) &= D d_0^\delta e^{-\lambda_0^* Dt}\int_0^{2\pi}\left(\rho\frac{d}{d\rho}v(\rho,\delta)\right)\Big|_{\rho=1} d\theta \\ &\sim 2\pi D d_0^\delta e^{-\lambda_0^* Dt}\nu A(\nu), \end{aligned} \tag{64}$$

where d_0^δ is given by

$$\begin{aligned} d_0^\delta &\sim c_0\int_{\Omega_0}\phi_0^*(\mathbf{x},\nu)d\mathbf{x} = -2\pi\nu A(\nu)c_0\int_{\Omega_0} G_{\lambda_0^*}(\mathbf{x};\mathbf{0})d\mathbf{x}, \\ &\sim -2\pi\nu A(\nu)c_0\int_{\Omega_0}\left(-\frac{1}{|\Omega_0|\lambda_0^*}+G_1(\mathbf{x};\mathbf{0})+\lambda_0^* G_2(\mathbf{x};\mathbf{0})\right)d\mathbf{x}, \\ &= \frac{2\pi\nu A(\nu)c_0}{\lambda_0^*}. \end{aligned}$$

Here, we have used (55) and (60) together with $\int_{\Omega_0} G_j d\mathbf{x} = 0$ for $j = 1, 2$. Substituting (58) for $A(\nu)$ into (64), yields

$$k^*(t) = \frac{D}{\lambda_0^*}\frac{c_0 e^{-\lambda_0^* Dt}}{\int_{\Omega_0}[G_{\lambda_0^*}(\mathbf{x};\mathbf{0})]^2 d\mathbf{x}}. \tag{65}$$

The integral appearing in (65) is evaluated in Appendix 2 with the result

$$\int_{\Omega_0} G_{\lambda_0^*}^2 d\mathbf{x} \sim \frac{1}{|\Omega_0|\lambda_0^{*2}}(1+\lambda_0^{*2}\mathcal{A}_1+\lambda_0^{*3}\mathcal{A}_2),$$

where the functions $\mathcal{A}_1 \equiv |\Omega_0| G_2(\mathbf{0};\mathbf{0})$ and $\mathcal{A}_2$ are given by (97) and (98), respectively. Thus, we get the final result

$$k^*(t) = \frac{c_0 |\Omega_0| D\lambda_0^*}{1 + \lambda_0^{*2}\mathcal{A}_1 + \lambda_0^{*3}\mathcal{A}_2} e^{-\lambda_0^* D t} \tag{66}$$

which should be compared with (47) for $k(t)$.

4 Numerical Simulations

In this section, we compare the reaction rates obtained from the three-term expansion (47) and from the infinite logarithmic expansion (66) with the results from the direct integration of the diffusion equation (4) on the domain Ω_δ using the *Partial Differential Equation Toolbox* of Matlab [17]. For the numerical simulations, we rescale all lengths by the length scale L of the cylindrical surface. In rescaled units the surface area and the gauge function $\nu(\delta)$ become

$$|\Omega_0^s| = \frac{4\pi R}{L}, \qquad \nu = \frac{1}{\log(L/\delta)}.$$

In the previous section it was shown that the reaction rate decays asymptotically in time as a single exponential function of the form

$$k(t) = Ae^{-\lambda t}. \tag{67}$$

Two different expressions for A and λ were derived. For the three-term expansion (47), $A \equiv A^{(3)}$ and $\lambda \equiv \lambda^{(3)}$ are given by

$$\begin{aligned} A^{(3)} &= c_0 L^2 |\Omega_0^s| \lambda^{(3)} \left(1 - \frac{4\pi^2 \nu^2}{|\Omega_0^s|} G_2(\mathbf{0};\mathbf{0})\right), \\ \lambda^{(3)} &= \frac{2\pi\nu D}{|\Omega_0^s| L^2} \left(1 - 2\pi\nu R_1(\mathbf{0};\mathbf{0}) + (2\pi\nu)^2 \left([R_1(\mathbf{0};\mathbf{0})]^2 - \frac{G_2(\mathbf{0};\mathbf{0})}{|\Omega_0^s|}\right)\right). \end{aligned} \tag{68}$$

In contrast, for the infinite logarithmic expansion (66), we set $A \equiv A^*$ and $\lambda \equiv \lambda^*$, where

$$A^* = \frac{c_0 L^2 |\Omega_0^s| \lambda^*}{(1 + \lambda_0^{*2}\mathcal{A}_1 + \lambda_0^{*3}\mathcal{A}_2)}, \quad \lambda^* = \frac{D}{L^2}\lambda_0^*. \tag{69}$$

Here, λ_0^* is given by (62). The functions $R_1(\mathbf{0};\mathbf{0})$, $G_2(\mathbf{0};\mathbf{0})$, $\mathcal{A}_1$ and $\mathcal{A}_2$ appearing above depend only on the aspect ratio L/R of the cylindrical surface. They are given by (91), (85), (97) and (98), respectively. All of these functions contain infinite series, e.g.

$$G_2(\mathbf{0};\mathbf{0}) = \frac{1}{4\pi}\left(\frac{1}{45}\frac{L}{R} + \frac{R}{L}\sum_{n=1}^{\infty}\frac{1}{n^2 \sinh^2(\frac{L}{R}n)} + \frac{R^2}{L^2}\sum_{n=1}^{\infty}\frac{\coth(\frac{L}{R}n)}{n^3}\right). \tag{70}$$

Numerical evaluation of these infinite sums shows that in the case of large aspect ratios $L/R \gg 1$ their contribution can be neglected, but for moderate aspect ratios such as $L/R \sim 5$ they contribute finite values. Thus, for numerical evaluation of these functions, the first term of each infinite series is retained, e.g. $G_2(\mathbf{0};\mathbf{0})$ is approximated by

$$G_2(\mathbf{0};\mathbf{0}) \approx \frac{1}{4\pi}\left(\frac{1}{45}\frac{L}{R} + \frac{R}{L}\frac{1}{\sinh^2(\frac{L}{R})} + \frac{R^2}{L^2}\coth\left(\frac{L}{R}\right)\right).$$

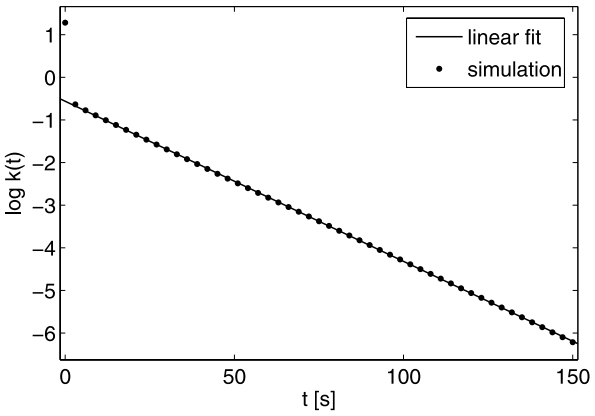

Fig. 2 Fit of a linear function to the logarithm of the reaction rate obtained from numerical simulations for $L/R = 5$ with $L = 2.5$ μm, $R = 0.5$ μm, $\delta = 0.05$ μm and $\lambda_{\text{sim}} = 0.0376\ \text{s}^{-1}$. Other parameters as in Table 1

As an application of our results, we consider the diffusion of IP_3R receptor ion channels on the membrane of the endoplasmic reticulum which forms a tubular network. The parameters are chosen as follows: The area of a tube is kept fixed at $|\Omega_0| = 5\pi\ \mu\text{m}^2$ while the aspect ratio L/R is varied in the range $5 \le L/R \le 80$ corresponding to $2.5\ \mu\text{m} \le L \le 10\ \mu\text{m}$ and $0.5\ \mu\text{m} \ge R \ge 0.125\ \mu\text{m}$. In this way, we can study the influence of the aspect ratio, i.e. the particular geometrical shape of the membrane, on the reaction rate of small diffusing molecules on its surface. The radius δ of an IP_3R receptor molecule is about 10 nm. The diffusion coefficient has been reported in the range $D = 0.02 \ldots 0.3\ \mu\text{m}^2\,\text{s}^{-1}$ [6, 8]. To test the validity of our approximations in (68) and (69) we also choose larger values of δ until substantial deviations from the numerical results are observed.

In the simulations we have set the initial condition to $c_0 = 1$. The simulations were continued for more than 100 seconds after the asymptotic regime had been reached. In general, the asymptotic regime begins when the initial perturbation, caused by the boundary layer, reaches the boundary of the cylindrical surface at $x = \pm L$. In our simulations we have observed that the asymptotic regime was reached on a time scale of order $L^2/4D$ which is the time scale of free diffusion in a (quasi-) one-dimensional space. Subsequently, the reaction rate decayed according to the exponential law (67).

The reaction rate was calculated from the flux to the absorbing boundary for each time step (every second). Subsequently, we fitted a simple linear function to the logarithm of the reaction rate from which the amplitude and the decay rate could be easily extracted according to (67). Two examples, corresponding to different aspect ratios and molecule sizes, are shown in Fig. 2 and Fig. 3 where the data points (dots) obtained from numerical simulations are plotted together with the linear fit (solid line). For a better visibility only every third data point is plotted. Note, that in the case $L/R = 80$, the asymptotic regime is reached after approximately 80 seconds (cf. Fig. 3) in agreement with the estimate given above.

The results of our simulations for two different aspect ratios L/R and three different molecule sizes δ are compiled in Table 1. This table also contains the theoretical values according to (68) and (69). As expected, if the aspect ratio is not too large, the three-term expansion ($A^{(3)}$, $\lambda^{(3)}$) and the infinite logarithmic expansion (A^*, λ^*) give equal results, although A^* is always closer to the value obtained from the full numerical computations than is $A^{(3)}$. However, for large aspect ratios and only moderately small values of δ the three-term expansion compares very poorly with full numerical results. In contrast, the infinite logarithmic expansion, which is intrinsically non-perturbative in character, shows excellent

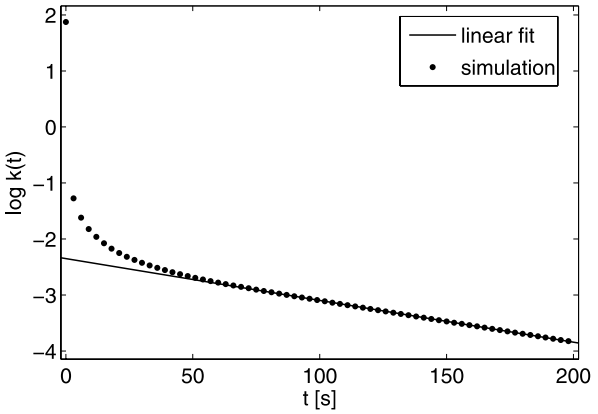

Fig. 3 Fit of a linear function to the logarithm of the reaction rate obtained from numerical simulations for $L/R = 80$ with $L = 10$ μm, $R = 0.125$ μm, $\delta = 0.1$ μm and $\lambda_{\text{sim}} = 0.0075\ \text{s}^{-1}$. Other parameters as in Table 1

Table 1 Comparison between the theoretically calculated reaction rates (68) and (69) and that obtained from numerical simulations for two different aspect ratios of the cylindrical surface L/R and fixed total area $|\Omega_0| = 5\pi\ \mu\text{m}^2$. Other parameters are: $D = 0.3\ \mu\text{m}^2\ \text{s}^{-1}$, $c_0 = 1\ \mu\text{m}^{-2}$

	$L/R = 80$			$L/R = 5$		
δ [μm]	0.01	0.05	0.1	0.01	0.05	0.1
λ_{sim}	0.0067	0.0072	0.0075	0.0252	0.0376	0.0478
λ^* [s^{-1}]	0.0067	0.0073	0.0076	0.0251	0.0376	0.0477
$\lambda^{(3)}$	0.0111	0.0203	0.0302	0.0251	0.0376	0.0478
A_{sim}	0.087	0.093	0.095	0.387	0.575	0.721
A^* [s^{-1}]	0.091	0.096	0.098	0.390	0.578	0.724
$A^{(3)}$	0.044	<0	<0	0.392	0.583	0.736

agreement with the results from numerical simulations even for large aspect ratios and relatively large molecule sizes.

From (67), the inverse decay rate $1/\lambda$ is a measure for the time scale over which the reaction rate has an appreciable strength. Figure 4 summarizes the dependence of the inverse decay rates $1/\lambda^{(3)}$ and $1/\lambda^*$ on the aspect ratio for a fixed value of the surface area $|\Omega_0| = 5\pi\ \mu\text{m}^2$ and $\delta = 0.01$ μm. This plot shows that for aspect ratios $L/R < 20$, the three-term expansion and the infinite logarithmic expansion yield basically identical results. In contrast, for aspect ratios larger than roughly $L/R = 60$, the three-term expansion underestimates the true decay rate. At small aspect ratios of $L/R \approx 3.1 \approx \pi$, the inverse decay rate exhibits a minimum showing that the reaction rate attains a maximum value in the case where the length of the cylindrical membrane approximately equals its circumference. Changing the radius δ of the diffusing molecules towards higher values, merely shifts the whole curves downwards, i.e. towards smaller inverse decay rates.

5 Discussion

We have calculated the reaction rate of small diffusing molecules on a cylindrical membrane. This study was motivated by the observation that IP_3R receptor channels form clusters on

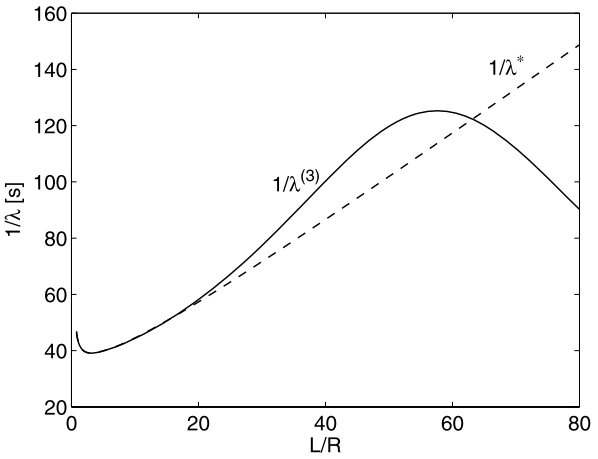

Fig. 4 Dependence of the inverse decay rates $1/\lambda^{(3)}$ (68) (*solid line*) and $1/\lambda^*$ (69) (*dashed line*) on the aspect ratio L/R for fixed surface area of the membrane $|\Omega_0| = 5\pi\ \mu\text{m}^2$. Other parameters are: $D = 0.3\ \mu\text{m}^2\,\text{s}^{-1}$, $\delta = 0.01\ \mu\text{m}$

the surface of the endoplasmic reticulum during ATP-induced calcium release from the ER. The ER is a tubular network of small interconnected cylindrical membrane parts. We have considered the reaction rate on one of the tubes by assuming that the net flux of receptor molecules across the boundaries between adjacent tubes is zero.

Our main results are (68) and (69), which have been derived using the method of matched asymptotic expansions. An alternative method, based on introducing pseudo-potential terms, was used in Ref. [23] to calculate eigenvalue corrections for some related problems. While (68) is correct up to terms of $\mathcal{O}(\nu^4)$ with $\nu^{-1} = \log L/\delta$, (69) is a generic non-perturbative result which contains all logarithmic corrections to the unperturbed eigenvalue and, therefore, should be correct up to transcendentally small terms of order $\mathcal{O}(\delta\nu(\delta))$. As shown in Table 1, the agreement of our results with those from numerical simulations is remarkably good.

The first order term

$$\lambda^{(1)} = \frac{2\pi D}{|\Omega_0|}\frac{1}{\log L/\delta}, \tag{71}$$

in the expression for the decay rate (41) only depends on the total area $|\Omega_0|$ of the cylindrical surface, but not on the specific geometry. Moreover, such a term can be derived only by matching the constant solution of the unperturbed problem (12) with the logarithmic singularity near the absorbing hole and thus, it should give the main contribution to the decay rate of small molecules (with circular cross section) in any bounded two-dimensional domain. In contrast, the higher order corrections explicitly depend on the aspect ratio L/R and therefore take into account the geometry of the membrane which is particularly important in the case of larger aspect ratios (cf. Table 1).

In the derivation of equations (68) and (69) it has been assumed that the absorbing molecule has a circular cross section and that it is located at the origin of the cylindrical surface. The first of these restrictions can be easily overcome. The only required modification to the analysis done in Sect. 3 is to replace the logarithmic gauge function with (cf. Ref. [24])

$$\frac{1}{\log L/\delta} \to \frac{1}{\log L/(d\delta)}, \tag{72}$$

where d is the logarithmic capacitance [18] depending on the shape of the small absorbing molecule. For example, in the case of an elliptical cross section, then $d = (a+b)/2$ where

a and b are the semi-axes of the ellipse. The second assumption has been made to facilitate the calculations and should be regarded as a first attempt to estimate the order of magnitude of the reaction rate on a finite two dimensional domain with the explicit dependence on the relevant system parameters. Preliminary numerical simulations have shown that the reaction rate can be significantly reduced if the reaction does not take place in the middle of the membrane (where $x = 0$). In biological systems, this can be achieved, for example, by the presence of anchor proteins located somewhere in the region $0 < x < L$ which can force the reaction to occur at a specific site of the membrane surface. The existence of such anchor proteins is discussed in Refs. [2, 6]. The direct interpretation of our numerical results for $x \neq 0$ is hampered by the fact that the asymptotic decay of the reaction rate appears to be multi-exponential. This indicates that the approximation made in (11) using only the dominant eigenmode φ_0^δ of the Helmholtz operator is no longer sufficient to describe the asymptotic behavior in that case.

To derive the reaction rate in (47) and (66) we have assumed no-flux boundary conditions which was motivated by biological considerations. In the original treatment by Smoluchowski the concentration of diffusing particles was kept fixed at spatial infinity to ensure a stationary reaction rate as $t \to \infty$ [21]. A similar treatment in our case would be to keep the concentration of diffusing channel proteins constant at the boundary of the cylindrical surface at $x = \pm L$. Such a situation might also be of biological relevance. Therefore, we have considered that problem in Appendix 3 where an asymptotic expansion for the stationary reaction rate is derived. The result reads

$$k_s = \frac{2\pi D \nu c_0}{1 + \nu R_s}, \quad \nu = \frac{1}{\log \frac{1}{\delta}}, \tag{73}$$

$$R_s = \frac{L}{2R} - \log \frac{L}{R} - 2\sum_{n=1}^{\infty} (-1)^n \log(1 - e^{-2\frac{L}{R}n}), \tag{74}$$

where the function R_s only depends on the aspect ratio L/R of the membrane. Note that this is also a non-perturbative result similar to the one in (69). It agrees excellently with results from numerical simulations up to aspect ratios of $L/R = 75$.

The experiments of Tateishi et al. [22] have shown that clustering of IP_3R receptor molecules on the ER membrane is a slow process in the order of tens of seconds. Typically, it took 50–60 seconds after the start of ATP stimulation in the extracellular domain before significant cluster formation could be observed. Since there is a certain delay until extracellular stimuli are translated into intracellular responses, the actual time scale of clustering is smaller than 50–60 s. To compare the experimental results with our calculations we note that the inverse decay rate λ^{-1} may serve as a measure of time for which the reaction rate (67) exhibits an appreciable strength before it decays to zero. The leading effect in the time scale is set by the ratio between the area $|\Omega_0|$ of the ER membrane and the diffusion coefficient D as well as the size δ of the receptor molecules (cf. (71)). In the case of IP_3R receptor ion channels ($\delta = 0.01$ μm) we find good agreement with experiments (see Fig. 4) for $D = 0.3\ \mu m^2\, s^{-1}$, $|\Omega_0| = 5\pi\ \mu m^2$ and aspect ratios in the range $5 \leq L/R \leq 15$ corresponding to $40\ s \leq \lambda^{-1} \leq 50\ s$ (cf. Fig. 4). However, our results are also compatible with a diffusion coefficient at the lower end of the reported range, e.g. $D = 0.06\ \mu m^2\, s^{-1}$, if the area of the membrane is accordingly reduced to $|\Omega_0| = \pi\ \mu m^2$. In this case, the aspect ratio of the membrane would have to be in the range $12 \leq L/R \leq 20$ to yield the same range of time scales as for the case $|\Omega_0| = 5\pi\ \mu m^2$.

In summary, our calculations support the view that receptor clustering on ER membranes with a moderate aspect ratio $L/R \leq 20$ might be a purely diffusion limited process. At the

same time it indicates that clustering can be faster than measured in the specific experiments above and therefore may have a role during intracellular Ca^{2+} oscillations in vivo [4, 5].

Finally, we mention that our results may be useful to estimate the reaction rate of receptor molecules on other intracellular organelles with a tubular shape such as cilia [7]. Also, the restriction to the case of simple diffusion in the calculation of the reaction rate is not a severe restriction. For example, our result can be readily applied to the case where free diffusion on the membrane is hampered by transient confinement zones such as lipid rafts where membrane receptor molecules may become trapped for some time before they can escape these domains and continue to perform free diffusion [3]. Such a process is still described by diffusion, i.e. it is a random walk between confinement domains, but on a coarse grained time scale.

Acknowledgements We would like to thank two anonymous reviewers for useful comments on the manuscript.

Appendix 1: Calculation of $R_1(\mathbf{0};\mathbf{0})$ and $G_2(\mathbf{0};\mathbf{0})$

In this appendix we derive the expressions for $R_1(\mathbf{0};\mathbf{0})$ and $G_2(\mathbf{0};\mathbf{0})$. For this purpose, we have to solve (30) and (35) with the boundary conditions (5), i.e.

$$\Delta G_1(\mathbf{x};\mathbf{0}) = \frac{1}{|\Omega_0|} - \delta(\mathbf{x}), \quad \mathbf{x} \in \Omega_0, \tag{75}$$

and

$$\Delta G_2 = -G_1, \quad \mathbf{x} \in \Omega_0. \tag{76}$$

For the following calculations, it will be convenient to measure all lengths in terms of the length scale L of the cylindrical surface, which is now given by

$$\Omega_0^s := \left\{ (x, y) : |x| \le 1, |y| \le \frac{\pi R}{L} \right\}. \tag{77}$$

In rescaled units we have $|\Omega_0^s| = 4\pi R/L$, while the boundary conditions for G_j with $j = 1, 2$ become

$$\begin{aligned} \partial_x G_j(\pm 1, y; \mathbf{0}) &= 0, \\ G_j\left(x, \frac{\pi R}{L}; \mathbf{0}\right) &= G_j\left(x, -\frac{\pi R}{L}; \mathbf{0}\right), \\ \partial_y G_j\left(x, \frac{\pi R}{L}; \mathbf{0}\right) &= \partial_y G_j\left(x, -\frac{\pi R}{L}; \mathbf{0}\right). \end{aligned} \tag{78}$$

In addition, G_1 and G_2 satisfy orthogonality relations of the form

$$\int_{\Omega_0^s} G_j(\mathbf{x};\mathbf{0}) d\mathbf{x} = 0, \quad j = 1, 2. \tag{79}$$

We look for a Fourier series representation of $G_1(\mathbf{x};\mathbf{0})$ on the domain Ω_0^s of (77). For this purpose, the delta function $\delta(\mathbf{x}) = \delta(x)\delta(y)$ is decomposed into Fourier modes as

$$\delta(x)\delta(y) = \left(\frac{1}{2} + \sum_{m=1}^{\infty} \cos(m\pi x) \right) \left(\frac{L}{2\pi R} + \frac{L}{\pi R} \sum_{n=1}^{\infty} \cos\left(\frac{nL}{R} y \right) \right).$$

Upon inserting this expression into (75), we obtain

$$\Delta G_1(\mathbf{x};\mathbf{0}) = -\frac{2}{|\Omega_0^s|}\left(\sum_{m=1}^{\infty}\cos(m\pi x)+\sum_{n=1}^{\infty}\cos\left(\frac{nL}{R}y\right)\right) - \frac{4}{|\Omega_0^s|}\sum_{m,n=1}^{\infty}\cos(m\pi x)\cos\left(\frac{nL}{R}y\right). \tag{80}$$

This shows that G_1 has the following Fourier series representation

$$G_1(\mathbf{x};\mathbf{0}) = \frac{2}{|\Omega_0^s|}\left(\frac{1}{\pi^2}\sum_{m=1}^{\infty}\frac{\cos(m\pi x)}{m^2}+\frac{R^2}{L^2}\sum_{n=1}^{\infty}\frac{\cos(\frac{nL}{R}y)}{n^2}\right) + \frac{2}{|\Omega_0^s|}\sum_{m,n=1}^{\infty}\frac{2\cos(m\pi x)\cos(\frac{nL}{R}y)}{(m\pi)^2+(\frac{nL}{R})^2}. \tag{81}$$

It is straightforward to confirm that this solution also satisfies the boundary conditions (78) as well as the orthogonality condition (79).

The solution G_2 to (76) can be calculated in a similar way. The result is

$$G_2(\mathbf{x};\mathbf{0}) = \frac{2}{|\Omega_0^s|}\left(\sum_{m=1}^{\infty}\frac{\cos(m\pi x)}{(\pi m)^4}+\sum_{n=1}^{\infty}\frac{\cos(\frac{nL}{R}y)}{(\frac{nL}{R})^4}\right) + \frac{2}{|\Omega_0^s|}\left(\sum_{m,n=1}^{\infty}\frac{2\cos(m\pi x)\cos(\frac{nL}{R}y)}{((m\pi)^2+(\frac{nL}{R})^2)^2}\right). \tag{82}$$

Now, $G_2(\mathbf{0},\mathbf{0})$ is readily evaluated by interchanging the infinite summations in (82) with the limiting procedure $\mathbf{x}\to\mathbf{0}$, since the resulting infinite series are absolutely convergent. As a result, we get

$$G_2(\mathbf{0},\mathbf{0}) = \frac{2}{|\Omega_0^s|}\left(\sum_{m=1}^{\infty}\frac{1}{(\pi m)^4}+\sum_{n=1}^{\infty}\frac{1}{(\frac{nL}{R})^2}+\sum_{m,n=1}^{\infty}\frac{2}{((\pi m)^2+(\frac{nL}{R})^2)^2}\right).$$

Making use of the well-known identities

$$\sum_{m=1}^{\infty}\frac{1}{m^4} = \frac{\pi^4}{90}, \tag{83}$$

$$\sum_{m=1}^{\infty}\frac{1}{(m^2+b^2)^2} = -\frac{1}{2b^4}+\frac{\pi^2}{4b^2\sinh^2(\pi b)}+\frac{\pi}{4b^3}\coth(\pi b), \tag{84}$$

we readily obtain

$$G_2(\mathbf{0};\mathbf{0}) = \frac{1}{4\pi}\left(\frac{1}{45}\frac{L}{R}+\frac{R}{L}\sum_{n=1}^{\infty}\frac{1}{n^2\sinh^2(\frac{L}{R}n)}+\frac{R^2}{L^2}\sum_{n=1}^{\infty}\frac{\coth(\frac{L}{R}n)}{n^3}\right). \tag{85}$$

The calculation of $R_1(\mathbf{0},\mathbf{0})$ is more difficult, since the double sum in (81) contains the logarithmic singularity of the Green's function, which has to be extracted before the limit

$\mathbf{x} \to \mathbf{0}$ can be applied. For the single sums in (81) the limit process can be interchanged with summation since the resulting series is absolutely convergent, e.g.

$$\lim_{x\to 0} \sum_{m=1}^{\infty} \frac{\cos(m\pi x)}{m^2} = \sum_{m=1}^{\infty} \frac{1}{m^2} = \frac{\pi^2}{6}. \tag{86}$$

The double sum will be computed in two steps. First, we perform the sum over 'm' using formula (1.445-2) from [11]

$$\sum_{k=1}^{\infty} \frac{\cos kx}{k^2 + b^2} = \frac{\pi}{2b} \frac{\cosh(b(\pi - x))}{\sinh(\pi b)} - \frac{1}{2b^2}, \quad 0 \le x \le 2. \tag{87}$$

Second, the resulting series over 'n' can be split into three parts one of which contains the logarithmic singularity while the other two give finite contributions in the limit $\mathbf{x} \to \mathbf{0}$.

The summation over 'm' in the double sum of (81) yields

$$\frac{2}{\pi^2} \sum_{m=1}^{\infty} \frac{\cos(m\pi x)}{(m)^2 + (\frac{nL}{\pi R})^2} = \frac{R}{Ln} \frac{\cosh((1-|x|)\frac{L}{R}n)}{\sinh(\frac{L}{R}n)} - \frac{R^2}{L^2 n^2}. \tag{88}$$

Upon using the double angle formula for $\cosh(x - y)$, together with

$$\coth x = 1 + \frac{2e^{-2x}}{1 - e^{-2x}}$$

and $\cosh x - \sinh x = e^{-x}$, the term in (88) containing the hyperbolic functions can be written as

$$\frac{\cosh((1-|x|)\frac{L}{R}n)}{\sinh(\frac{L}{R}n)} = e^{-\frac{L}{R}|x|n} + \frac{2e^{-2\frac{L}{R}n}}{1 - e^{-2\frac{L}{R}n}} \cosh\left(\frac{L}{R}nx\right). \tag{89}$$

The subsequent summation over 'n', given by

$$\begin{aligned} &\sum_{n,m=1}^{\infty} \frac{2\cos(m\pi x)\cos(\frac{nL}{R}y)}{(m\pi)^2 + (\frac{nL}{R})^2} \\ &= \frac{R}{L} \sum_{n=1}^{\infty} \frac{e^{-\frac{L}{R}|x|n} \cos(\frac{L}{R}ny)}{n} + \frac{R}{L} \sum_{n=1}^{\infty} \frac{1}{n} \frac{2e^{-2\frac{L}{R}n}}{1 - e^{-2\frac{L}{R}n}} \cosh\left(\frac{L}{R}nx\right) \cos\left(\frac{L}{R}ny\right) \\ &\quad - \frac{R^2}{L^2} \sum_{n=1}^{\infty} \frac{\cos(\frac{L}{R}ny)}{n^2}, \end{aligned} \tag{90}$$

shows that the last sum precisely cancels the second (single) sum in (81). The first sum in (90) is readily evaluated when the cosine function is written as a sum of two exponentials and the power series expansion of the logarithm $\sum_{k=1}^{\infty} k^{-1} z^k = -\log(1 - z)$ for $|z| < 1$ is used. In this way, we get

$$\frac{R}{L} \sum_{n=1}^{\infty} \frac{\cos(\frac{nL}{R}y)}{n} e^{-\frac{|x|L}{R}n} = -\frac{R}{2L} \log\{(1 - e^{-\frac{L}{R}(|x|+iy)})(1 - e^{-\frac{L}{R}(|x|-iy)})\}.$$

The small argument expansion of the exponential functions then yields

$$\begin{aligned}
&-\frac{R}{2L}\lim_{\mathbf{x}\to\mathbf{0}}\log\{(1-e^{-\frac{L}{R}(|x|+iy)})(1-e^{-\frac{L}{R}(|x|-iy)})\}\\
&\quad=-\frac{R}{2L}\lim_{\mathbf{x}\to\mathbf{0}}\log\left\{\left(\frac{L^2}{R^2}(x^2+y^2)\right)(1-\mathcal{O}(|x|,y^2))\right\}\\
&\quad=-\frac{R}{L}\log\frac{L}{R}-\frac{R}{L}\log\sqrt{x^2+y^2}.
\end{aligned}$$

It remains to evaluate the second sum (90) in the limit $\mathbf{x}\to\mathbf{0}$. In the calculation, a series of Lambert type [14] is obtained

$$\sum_{n=1}^{\infty}\frac{1}{n}\frac{q^n}{1-q^n},\quad q\equiv e^{-2\frac{L}{R}}<1,$$

which may be rewritten as

$$\sum_{n=1}^{\infty}\frac{q^n}{n(1-q^n)}=\sum_{n=1}^{\infty}\frac{q^n}{n}\sum_{m=0}^{\infty}(q^n)^m=\sum_{m=0}^{\infty}\sum_{n=1}^{\infty}\frac{(q^{m+1})^n}{n}=-\sum_{m=1}^{\infty}\log(1-q^m).$$

Since the Lambert series is absolutely convergent [14], the two limiting processes can, again, be interchanged yielding

$$\begin{aligned}
&\lim_{\mathbf{x}\to\mathbf{0}}\frac{R}{L}\sum_{n=1}^{\infty}\frac{1}{n}\frac{2e^{-2\frac{L}{R}n}}{1-e^{-2\frac{L}{R}n}}\cosh\left(\frac{L}{R}nx\right)\cos\left(\frac{L}{R}ny\right)\\
&\quad=\frac{R}{L}\sum_{n=1}^{\infty}\frac{1}{n}\frac{2e^{-2\frac{L}{R}n}}{1-e^{-2\frac{L}{R}n}}=-2\frac{R}{L}\sum_{n=1}^{\infty}\log(1-e^{-2\frac{L}{R}n}).
\end{aligned}$$

In summary, we obtain upon also recalling (86), that for $\mathbf{x}\to 0$ the Green's function $G_1(\mathbf{x};\mathbf{0})$ behaves like

$$\begin{aligned}
\lim_{\mathbf{x}\to 0}G_1(\mathbf{x};\mathbf{0})&=\frac{2L}{4\pi R}\left(\frac{1}{\pi^2}\frac{\pi^2}{6}-\frac{R}{L}\log\frac{L}{R}-\frac{R}{L}\log\sqrt{x^2+y^2}\right)\\
&\quad+\frac{2L}{4\pi R}\left(-2\frac{R}{L}\sum_{n=1}^{\infty}\log(1-e^{-2\frac{L}{R}n})\right),\\
&=-\frac{1}{2\pi}\log|\mathbf{x}|+\frac{L}{12\pi R}-\frac{1}{2\pi}\log\frac{L}{R}-\frac{1}{\pi}\sum_{n=1}^{\infty}\log(1-e^{-2\frac{L}{R}n}).
\end{aligned}$$

From this expression the regular part of the Green's function given by (31) can be read off as

$$R_1(\mathbf{0};\mathbf{0})=\frac{1}{2\pi}\left(\frac{L}{6R}-\log\left(\frac{L}{R}\right)-2\sum_{n=1}^{\infty}\log(1-e^{-2nL/R})\right).\tag{91}$$

Note that $R_1(\mathbf{0};\mathbf{0})$ depends only on the aspect ratio L/R. In particular, for large aspect ratios one can safely approximate $R_1(\mathbf{0};\mathbf{0})$ by the first two terms, and neglect the infinite sum

of logarithmic corrections. As a remark, if we had interchanged the order of summation in the double sum in (81), and had instead begun with the summation over 'n', while following the remainder of the calculation above, we would have obtained a different representation of the regular part $R_1(\mathbf{0};\mathbf{0})$ of the Green's function in (81), namely

$$R_1(\mathbf{0};\mathbf{0}) = \frac{1}{2\pi}\left(\frac{\pi^2 R}{6L} - \log\pi - 2\sum_{n=1}^{\infty}\log(1-e^{-2\pi^2 nR/L})\right). \tag{92}$$

One may readily show that both expressions yield the same numerical value, but with a different speed of convergence. While (91) converges rapidly for $L/R \gg 1$, the other representation performs better if $L/R \ll \pi^2$. Hence, there is an overlap region where both expressions are equally good (or bad). For example, if $L/R = 5$ only one term of the sum in (91) and three terms of the sum in (92) are needed to give the same result with an accuracy of 6 digits. In contrast, if $L/R = 25$ then twenty terms of the sum in (92) and no term from the sum in (91) are needed to achieve the same accuracy.

Appendix 2: Calculation of the Integral Appearing in (65)

In this section, we will use the Fourier series representations for G_1 and G_2, given by (81) and (82), respectively, to calculate the integral appearing in (65) for the reaction rate $k^*(t)$:

$$\int_{\Omega_0^s}[G_{\lambda^*}(\mathbf{x};\mathbf{0})]^2 d\mathbf{x} = \int_{\Omega_0^s}\left(-\frac{1}{|\Omega_0^s|\lambda_0^*} + G_1(\mathbf{x};\mathbf{0}) + \lambda_0^* G_2(\mathbf{x};\mathbf{0})\right)^2 d\mathbf{x}. \tag{93}$$

The main contribution arises from the constant term, i.e.

$$\int_{\Omega_0^s}\frac{1}{|\Omega_0^s|^2\lambda_0^{*2}}d\mathbf{x} = \frac{1}{|\Omega_0^s|\lambda_0^{*2}}. \tag{94}$$

Due to the orthogonality relations (79), the terms linear in G_1 and G_2 vanish. Therefore, it remains to evaluate

$$\int_{\Omega_0^s}(G_1+\lambda_0^* G_2)^2 d\mathbf{x} \sim \int_{\Omega_0^s}(G_1^2 + 2\lambda_0^* G_1 G_2)d\mathbf{x}, \tag{95}$$

where we have again neglected terms quadratic in λ_0^*. Upon recalling the orthogonality relations of the trigonometric functions

$$\int_{-1}^{1}\cos(\pi m x)dx = \int_{-\frac{\pi R}{L}}^{\frac{\pi R}{L}}\cos\left(\frac{nL}{R}y\right)dy = 0,$$

$$\int_{-1}^{1}\cos(\pi m x)\cos(\pi n x)dx = \delta_{mn},$$

$$\int_{-\frac{\pi R}{L}}^{\frac{\pi R}{L}}\cos\left(\frac{mL}{R}y\right)\cos\left(\frac{nL}{R}y\right)dy = \frac{\pi R}{L}\delta_{mn},$$

we obtain for the first term in (95) that

$$\int_{\Omega_0^s} G_1^2 d\mathbf{x} = \frac{4}{|\Omega_0^s|^2}\left(\frac{|\Omega_0^s|}{2\pi^4}\sum_{m=1}^{\infty}\frac{1}{m^4} + \frac{|\Omega_0^s|}{2}\frac{R^4}{L^4}\sum_{m=1}^{\infty}\frac{1}{m^4}\right) \tag{96}$$

$$+ \frac{4}{|\Omega_0^s|^2}\left(\frac{|\Omega_0^s|}{\pi^4}\sum_{m,n=1}^{\infty}\frac{1}{(m^2+(\frac{nL}{\pi R})^2)^2}\right)$$

$$= \frac{1}{|\Omega_0^s|}\left(\frac{1}{45} + \frac{R^2}{L^2}\sum_{n=1}^{\infty}\frac{1}{n^2\sinh^2(\frac{L}{R}n)} + \frac{R^3}{L^3}\sum_{n=1}^{\infty}\frac{\coth(\frac{L}{R}n)}{n^3}\right)$$

$$\equiv \frac{\mathcal{A}_1}{|\Omega_0^s|} \tag{97}$$

while the second integral becomes

$$2\int_{\Omega_0^s} G_1 G_2 d\mathbf{x} = \frac{1}{|\Omega_0^s|}\left(\frac{4}{945} + \frac{3}{2}\frac{R^4}{L^4}\sum_{n=1}^{\infty}\frac{1}{n^4\sinh^2(\frac{L}{R}n)} + \frac{3}{2}\frac{R^5}{L^5}\sum_{n=1}^{\infty}\frac{\coth(\frac{L}{R}n)}{n^5}\right)$$

$$+ \frac{1}{|\Omega_0^s|}\left(\frac{R^3}{L^3}\sum_{n=1}^{\infty}\frac{\coth(\frac{L}{R}n)}{n^3\sinh^2(\frac{L}{R}n)}\right)$$

$$\equiv \frac{\mathcal{A}_2}{|\Omega_0^s|}. \tag{98}$$

Here, we have used

$$\sum_{m=1}^{\infty}\frac{1}{m^6} = \frac{\pi^6}{945}, \tag{99}$$

together with (84) and formula (6.1.174) from [12]

$$\sum_{m=1}^{\infty}\frac{1}{(m^2+b^2)^3} = -\frac{1}{2b^6} + \frac{3\pi}{16b^5}\coth(\pi b) + \frac{3\pi^2}{16b^4\sinh^2(\pi b)}$$

$$+ \frac{\pi^3\coth(\pi b)}{8b^3\sinh^2(\pi b)}.$$

In summary, this analysis shows that

$$\int_{\Omega_0^s}[G_{\lambda^*}(\mathbf{x};\mathbf{0})]^2 d\mathbf{x} \sim \frac{1}{|\Omega_0^s|\lambda_0^{*2}}(1+\lambda_0^{*2}\mathcal{A}_1 + \lambda_0^{*3}\mathcal{A}_2). \tag{100}$$

Appendix 3: Stationary Reaction Rate

We calculate the stationary reaction rate of small diffusing molecules on a cylindrical surface which is reached after sufficiently long time when the initial concentration is kept fixed at the boundary of the cylindrical surface. The calculation is very similar to the case of no-flux

boundary conditions discussed at length in Sect. 3. Therefore, we give here only the main steps of the derivation.

We look for the stationary solution of the diffusion equation (4) in the scaled domain Ω_0^δ (see (77)), i.e. we consider the following BVP

$$\begin{aligned} \Delta c = 0, \qquad c(\mathbf{x}) = 0 \quad \text{at } |\mathbf{x}| = \delta, \\ c(\pm 1, y) = c_0, \end{aligned} \tag{101}$$

and periodic boundary conditions in the y-direction. Here, c_0 is the initial concentration which is kept fixed at the boundary of the cylinder at $x = \pm 1$. To solve this BVP we introduce asymptotic expansions as in Sect. 3.5

$$c_{out} = \Phi(\mathbf{x}, \nu) + \sigma(\delta)\Psi(\mathbf{x}), \quad |\mathbf{x}| \sim \mathcal{O}(1), \tag{102}$$

$$c_{in} = \nu A(\nu) \log|\mathbf{y}| + \mathcal{O}(\delta), \quad |\mathbf{y}| = |\mathbf{x}|/\delta = \mathcal{O}(1), \tag{103}$$

where $\sigma \ll \nu^k$ for any $k \geq 1$ and $\nu = -1/\log\delta$. The function $\Phi(\mathbf{x})$ contains all logarithmic corrections to the solution of the unperturbed problem while $A(\nu)$ has to be found from matching the inner and outer expansions. Rewriting the inner expansion c_{in} in terms of outer variables yields the matching condition

$$\lim_{\mathbf{x}\to\mathbf{0}} \Phi(\mathbf{x}, \nu) = A(\nu) + \nu A(\nu) \log|\mathbf{x}|. \tag{104}$$

This reveals that Φ has a logarithmic singularity at the origin. Using the outer expansion c_{out} in the BVP (101) shows that Φ has to be a solution of the equation

$$\Delta\Phi = 2\pi\nu A(\nu)\delta(\mathbf{x}) \tag{105}$$

where we have added a delta function to account for the correct singularity behavior in a similar way as in Sect. 3. The solution to this equation can be decomposed as $\Phi(\mathbf{x}, \nu) = \Phi_0(\mathbf{x}) - 2\pi\nu A(\nu) G(\mathbf{x}; \mathbf{0})$ where Φ_0 is a solution of the unperturbed problem

$$\Delta\Phi_0 = 0, \qquad \Phi_0(\pm 1, y) = c_0 \tag{106}$$

and G is a Green's function satisfying

$$\Delta G = -\delta(\mathbf{x}), \qquad G(\pm 1, y) = 0 \tag{107}$$

together with periodic boundary conditions in the y-direction. From the singularity behavior of the Green's function

$$\lim_{\mathbf{x}\to\mathbf{0}} G = -\frac{1}{2\pi}(\log|\mathbf{x}| - R_0), \tag{108}$$

and the matching condition equation (104), the function $A(\nu)$ is determined by

$$\begin{aligned} \lim_{\mathbf{x}\to\mathbf{0}} \Phi(\mathbf{x}, \nu) &= A(\nu) + \nu A(\nu) \log|\mathbf{x}| \\ &\stackrel{!}{=} \Phi_0(\mathbf{0}) + 2\pi\nu A(\nu)\frac{1}{2\pi}(\log|\mathbf{x}| - R_0). \end{aligned}$$

Solving for $A(\nu)$ yields

$$A(\nu) = \frac{\Phi_0(\mathbf{0})}{1 + \nu R_0}, \tag{109}$$

where R_0 is the regular part of the Green's function G. The stationary reaction rate k_s is then calculated as the flux towards the small absorbing hole at $|\mathbf{y}| = 1$ (cf. (1)). Using the inner expansion in (103) we obtain

$$k_s = 2\pi D\nu \frac{\Phi_0(\mathbf{0})}{1+\nu R_0}. \tag{110}$$

The constant $\Phi_0(\mathbf{0})$ is determined by the solution to the unperturbed problem (106) which is simply given by $\Phi_0 \equiv c_0$. The Green's function in (107) can be found in a similar way as in Appendix 1 using the Fourier representation of the δ-function (with $|\Omega_0^s| = 4\pi R/L$)

$$\delta(\mathbf{x}) = \frac{1}{|\Omega_0^s|}\left(1 + 2\sum_{m=1}^{\infty}\cos[m\pi x] + 2\sum_{n=1}^{\infty}\cos\left[\frac{nL}{R}y\right]\right) + \frac{4}{|\Omega_0^s|}\left(\sum_{m,n=1}^{\infty}\cos[m\pi x]\cos\left[\frac{nL}{R}y\right]\right).$$

A particular solution of (107) is given by

$$G = \frac{1}{|\Omega_0^s|}\left(-\frac{x^2}{2} + \frac{2}{\pi^2}\sum_{m=1}^{\infty}\frac{\cos[m\pi x]}{m^2} + 2\frac{R^2}{L^2}\sum_{n=1}^{\infty}\frac{\cos[\frac{nL}{R}y]}{n^2}\right) + \frac{4}{|\Omega_0^s|}\sum_{m,n=1}^{\infty}\frac{\cos[m\pi x]\cos[\frac{nL}{R}y]}{(m\pi)^2 + (\frac{nL}{R})^2}.$$

While this function is periodic in the y-direction it does not fulfill the boundary condition in (107). Instead, we obtain

$$\lim_{x\to\pm 1} G = \frac{1}{|\Omega_0^s|}\left(-\frac{1}{2} - \frac{1}{6} + 2\frac{R}{L}\sum_{n=1}^{\infty}\frac{\cos[\frac{nL}{R}y]}{n\sinh[\frac{nL}{R}]}\right).$$

Thus, we have to find a harmonic function H satisfying

$$\lim_{x\to\pm 1} H = \frac{1}{|\Omega_0^s|}\left(\frac{2}{3} - 2\frac{R}{L}\sum_{n=1}^{\infty}\frac{\cos[\frac{nL}{R}y]}{n\sinh[\frac{nL}{R}]}\right),$$

such that $\lim_{x\to\pm 1}(G+H) = 0$. This function is given by

$$H = \frac{1}{|\Omega_0^s|}\left(\frac{2}{3} - 2\frac{R}{L}\sum_{n=1}^{\infty}\frac{\cosh[\frac{nL}{R}x]\cos[\frac{nL}{R}y]}{n\cosh[\frac{nL}{R}]\sinh[\frac{nL}{R}]}\right),$$

and the general solution to (107) reads

$$G = \frac{1}{|\Omega_0^s|}\left(-\frac{x^2}{2} + \frac{2}{3} + \frac{2}{\pi^2}\sum_{m=1}^{\infty}\frac{\cos[m\pi x]}{m^2} + 2\frac{R^2}{L^2}\sum_{n=1}^{\infty}\frac{\cos[\frac{nL}{R}y]}{n^2}\right) + \frac{1}{|\Omega_0^s|}\left(4\sum_{m,n=1}^{\infty}\frac{\cos[m\pi x]\cos[\frac{nL}{R}y]}{(m\pi)^2 + (\frac{nL}{R})^2} - 4\frac{R}{L}\sum_{n=1}^{\infty}\frac{\cosh[\frac{nL}{R}x]\cos[\frac{nL}{R}y]}{n\sinh[2\frac{nL}{R}]}\right).$$

In the limit $\mathbf{x} \to \mathbf{0}$ the Green's function G behaves like

$$\lim_{\mathbf{x}\to\mathbf{0}} G = \frac{L}{4\pi R}\left(1 - 2\frac{R}{L}\log\frac{L}{R} - 2\frac{R}{L}\log|\mathbf{x}| - 4\frac{R}{L}\sum_{n=1}^{\infty}(-1)^n \log(1 - e^{-2\frac{L}{R}n})\right),$$

which shows that its regular part appearing in (110) is given by

$$R_0 = \frac{L}{2R} - \log\frac{L}{R} - 2\sum_{n=1}^{\infty}(-1)^n \log(1 - e^{-2\frac{L}{R}n}). \tag{111}$$

In deriving this equation we made use of (90) and

$$\sum_{n=1}^{\infty}\frac{1}{n\sinh[2\frac{nL}{R}]} = 2\sum_{n=1}^{\infty}\frac{1}{n}\frac{e^{-2\frac{L}{R}n}}{1 - e^{-4\frac{L}{R}n}} = 2\sum_{m=0}^{\infty}\sum_{n=1}^{\infty}\frac{(e^{-(2m+1)2\frac{L}{R}})^n}{n}$$

$$= -2\sum_{m=0}^{\infty}\log(1 - e^{-(2m+1)2\frac{L}{R}}).$$

References

1. Berg, H.C., Purcell, E.M.: Physics of chemoreception. Biophys. J. **20**, 193–219 (1977)
2. Chalmers, M., Schell, M., Thorn, P.: Agonist-evoked inositol trisphosphate receptor IP_3R clustering is not dependent on changes in the structure of the endoplasmic reticulum. Biochem. J. **394**(1), 57–66 (2006)
3. Dietrich, C., Yang, B., Fujiwara, T., Kusumi, A., Jacobson, K.: Relationship of lipid rafts to transient confinement zones detected by single particle tracking. Biophys. J. **82**, 274–284 (2002)
4. Falcke, M.: Reading the patterns in living cells—the physics of Ca^{2+} signaling. Adv. Phys. **53**(3), 255–440 (2004)
5. Falcke, M., Malchow, D. (eds.): Understanding Calcium Dynamics. Lecture Notes in Physics. Springer, Berlin (2003)
6. Ferreri-Jacobia, M., Mak, D.D., Foskett, J.K.: Translational mobility of the type 3 inositol 1,4,5-trisphosphate receptor Ca^{2+} release channel in endoplasmic reticulum membrane. J. Biol. Chem. **280**, 3824–3831 (2005)
7. Flannery, R.J., French, D.A., Kleene, S.J.: Clustering of cyclic-nucleotide-gated channels in olfactory cilia. Biophys. J. **91**(1), 179–188 (2006). DOI: 10.1529/biophysj.105.079046. URL: http://www.biophysj.org/cgi/content/abstract/91/1/179
8. Fukatsu, K., Bannai, H., Zhang, S., Nakumara, H., Inoue, T., Mikoshiba, K.: Lateral diffusion of inositol 1,4,5-trisphosphate receptor type 1 is regulated by actin filaments and 4.1n in neutonal dendrites. J. Biol. Chem. **279**(47), 48,976–48,982 (2004)
9. Goldstein, B., Posner, R.G., Torney, D.C., Erickson, J., Holowka, D., Baird, B.: Competition between solution and cell surface receptors for ligand. Biophys. J. **56**, 955–966 (1989)
10. Gopalakrishnan, M., Forsten-Williams, K., Nugent, M.A., Täuber, U.C.: Effects of receptor clustering on ligand dissociation kinetics: theory and simulations. Biophys. J. **89**, 3686–3700 (2005)
11. Gradshteyn, I.S., Ryzhik, I.M.: Tables of Integrals, Series and Products. Academic Press, New York (1965)
12. Hansen, E.R.: A Table of Series and Products. Prentice-Hall, New Jersey (1975)
13. Kevorkian, J., Cole, J.D.: Multiple Scale and Singular Perturbation Methods. Springer, New York (1996)
14. Knopp, K.: Theorie und Anwendung der Unendlichen Reihen. Springer, Berlin (1964)
15. Lange, C., Weinitschke, H.: Singular perturbations of elliptic problems on domains with small holes. Stud. Appl. Math. **92**, 55–93 (1994)
16. Larsen, A.Z., Kummer, U.: Information processing in calcium signal transduction. In: Falcke, M., Malchow, D. (eds.) Understanding Calcium Dynamics. Lecture Notes in Physics, pp. 153–178. Springer, Berlin (2003)
17. Matlab: Partial Differential Equation Toolbox, User's Guide. The Mathworks, Natick (1996)

18. Ransford, T.: Potential Theory in the Complex Plane. Cambridge University Press, Cambridge (1995)
19. Redner, S.: A Guide to First-Passage Processes. Cambridge University Press, Cambridge (2001)
20. Shoup, D., Szabo, A.: Role of diffusion in ligand binding to macromolecules and cell-bound receptors. Biophys. J. **40**, 33–39 (1982)
21. v. Smoluchowski, M.: Versuch einer mathematischen Theorie der Koagulationskinetik kolloider Lösungen. Z. Phys. Chem. **92**, 129–168 (1917)
22. Tateishi, Y., Hattori, M., Nakayama, T., Iwai, M., Bannai, H., Nakamura, T., Michikawa, T., Inoue, T., Mikoshiba, K.: Cluster formation of inositol 1,4,5-trisphosphate recepter requires its transition to open state. J. Biol. Chem. **280**(8), 6816–6822 (2005)
23. Torney, D.C., Goldstein, B.: Rates of diffusion limited reaction in periodic systems. J. Stat. Phys. **49**(3), 725–750 (1987)
24. Ward, M.J.: Diffusion and bifurcation problems in singularly perturbed domains. Nat. Resour. Model. **13**(2), 271–302 (2000)
25. Ward, M.J., Henshaw, W.D., Keller, J.B.: Summing logarithmic expansions for singularly perturbed eigenvalue problems. SIAM J. Appl. Math. **53**(3), 799–828 (1993)